Define Minimum Safe Operational Volume for Aerial Vehicles in Upper Class E Airspace

Min Xue*
NASA Ames Research Center, Moffett Field, CA 94035

Abraham K. Ishihara†
KBR Wyle Services, LLC. NASA Ames Research Center, Moffett Field, CA 94035

The variety of vehicle performance in upper Class E airspace requires a method that can efficiently compute the minimum safe operational boundary between aircraft. This work presents a mathematical method to define the minimum safe operational boundary needed for aerial vehicles operating in upper Class E airspace. This method focuses on the extra separation required by vehicle maneuverability, communication delay, and control/operator response time. A sensitivity study is then performed to provide a general understanding of the impact of these factors on the extra separation needed. Experiments with pairwise encounters are conducted to verify the results generated by the proposed methods.

I. Introduction

High altitude operations above 60,000 feet allow broader service area coverage than at ground level and have attracted many commercial applications. Balloons [1], airships [2], and high altitude long endurance (HALE) high-aspect-ratio wing aerial vehicles [3, 4] have been developed to provide platforms to enable these high-altitude operations. Many existing military and scientific operations make use of high altitude airspace, and future supersonic commercial operations [5, 6] are envisioned to use these higher altitudes as well. As stated in the FAA upper Class E Traffic Management (ETM) concept of operations [7], the increasing demand of upper Class E operations, combined with disparate vehicle performance characteristics, present a great challenge to currently limited airspace management service in upper Class E. While the concept of cooperative operations is prevalent among ETM stakeholders [7–9], defining the minimum safe operational boundary remains as the first critical task to enable successful upper Class E operations.

The minimum safe operational boundary refers to the safe boundary between two aerial vehicles, within which the violation of separation becomes inevitable. Many factors contribute to the minimum safe operational boundary shown as multiple-layer rings in Fig. 1. The first layer is caused by the error of the intruder's relative position acquired by the ownship aerial vehicle. Depending on the approach that the ownship applied to obtain the relative position of the intruder, errors may originate from a vehicle-to-vehicle communication like ADS-B, navigation system, or onboard or ground-based radars. When there are multiple sources for position information, data fusion algorithms may be applied to reduce the errors. The second layer protects both ownship and intruder aircraft from the wake, vortex, or pressure fluctuation generated by the other aircraft. Although the vortex-induced separation typically applies when an aircraft is trailing another aircraft in current manned aviation, it may also apply in different situations in upper Class E operations. For instance, when a fixed-wing aircraft passes by a balloon or airship, or when a supersonic aircraft passes by a HALE aircraft, these HALE vehicles might be sensitive to the wake, vortex, or air pressure fluctuation within a certain range. The third factor is the limited maneuverability of the ownship. Because the aircraft cannot instantaneously change its heading, speed, or altitude, extra space and time are needed for such a transition. The fourth factor is the information update rate, which refers to the interval between two consecutive intruder positions/states acquired by the ownship. The fifth factor is the control response time, which is defined as the time needed from when the information is acquired to when a resolution is executed. The response time could vary due to the actions of remote pilots in many ETM vehicles. The separation required by the first two factors is decided by position acquisition and aerodynamics, and they can be measured separately. For simplicity, the separation required by these two factors is assumed to be a constant in this work and will be called minimum separation through this paper. This work focuses on the latter three factors as their impact is more dynamic.

*Aerospace Research Engineer, Aviation Systems Division. Mail Stop 210-15. AIAA senior member.
†Aerospace Research Scientist, KBR Wyle Services, LLC. AIAA member

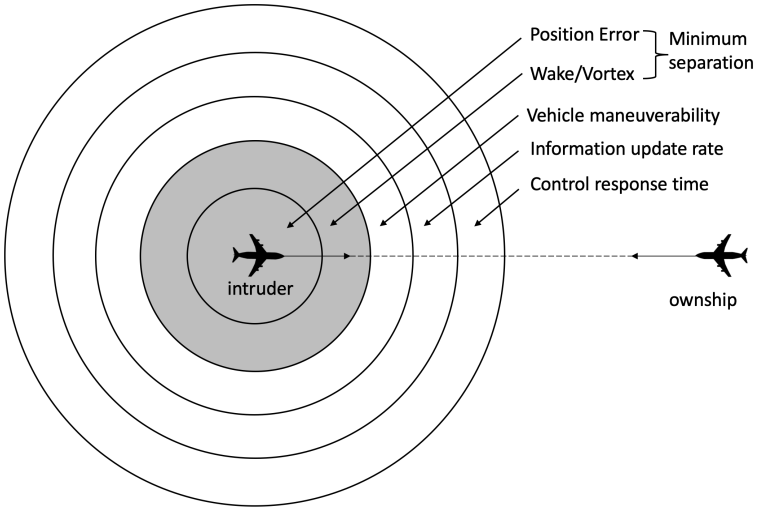

Fig. 1 Factors contributing to the minimum safe operational boundary

Recently, there has been much research on well-clear definition - a definition similar to the minimum safe operational boundary caused by maneuverability - for large and small UAVs [10–13]. The typical approach adopted in those studies is: scenarios were first generated either based on predicted missions [10, 11] or using millions of complementary pairwise encounters [12]; then several predefined candidate definitions were examined with simulations, which often include radar and communication models, to quantify the risks and identify the best candidate. However, there are two main drawbacks of this type of approach. First, they are only suitable for finding a one-size-fits-all well-clear definition, and given the diversity of the vehicle performance in upper Class E operations, a dynamic minimum safe operational boundary will be necessary for different encounter scenarios. Second, candidate definitions are provided based on past experiences. For the wide range of upper Class E vehicles, it would not be plausible and efficient to generate the number of initial guesses of candidate definitions needed for various encounter situations prior to running experiments. Therefore, developing a more versatile method to define the minimum safe operational boundary for different encounter situations is necessary. Meanwhile, the method can also help understand the impact and sensitivity of these factors and to provide accurate estimations prior to simulations.

This work develops a mathematical method to define the minimum safe operational boundary considering vehicle maneuverability, information update rate, and response delays. A sensitivity study of these factors is presented to obtain a fundamental understanding of their impacts on the buffer size. Finally, selected results are verified using simulations. The paper is organized as follows: Section II presents the methods and demonstrative results. Section III shows the sensitivity of the minimum safe boundary to several key parameters. Section IV uses simulations with different encounter scenarios to verify a selected safe boundary calculated using the proposed algorithm. Section V concludes this work.

II. Method

Assuming the minimum separation mandated by the position error and wake vortex considerations is a known constant, this section presents a mathematical method for the other three factors: vehicle maneuverability, information update interval and control response delay. Section II.A describes the method for extra separation required by vehicle maneuverability, and Section II.B shows the method for separation needed by information update interval and control response delay.

A. Separation Required by Vehicle Maneuverability

A mathematical method is proposed in this subsection to compute the boundary caused by the vehicle maneuverability. Mathematical methods have been developed in the past to address the separation caused by vehicle maneuverability. Tomlin et al. [14] calculated the minimal unsafe operating region for an aircraft with angular and linear velocities as control actions, respectively. A Hamilton-Jacobi-Isaacs equation was constructed based on a relative aircraft

configuration model to identify the minimal unsafe operating region. However, the computation of the boundary is in general difficult. Duffield et al. [13] derived an analytical solution only for the worst case where two vehicles are in a head-on situation. Although the calculation is efficient, a comprehensive understanding of the separation mandated by vehicle maneuverability is needed. This work proposes an efficient method that uses the kinetic vehicle model and simple optimization to identify the complete minimum safe operational boundary needed due to the limit of vehicle maneuverability. In this work, the horizontal heading change or angular velocity is assumed to be the conflict resolution maneuver option.

1. Algorithm

Assuming v_o and ψ_o are the magnitude and direction of ownship's velocity, respectively and v_i and ψ_i are the magnitude and direction for intruder's velocity, respectively, for any turn rate ω of the ownship, the relative velocity vector $\vec{V}_r$ (relative to the intruder) can be expressed as Eqn. 1. For simplicity, v_o, v_i, ψ_o, and ψ_i will not be shown as arguments on the left side of the following equations.

$$\vec{V}_r(\omega, t) = \begin{bmatrix} v_o \sin(\psi_o + \omega t) - v_i \sin\psi_i \\ v_o \cos(\psi_o + \omega t) - v_i \cos\psi_i \end{bmatrix} \tag{1}$$

The relative distance to the intruder at any given time would be a function shown in Eqn. 2 for any given d_r and θ_r, where d_r and θ_r are the magnitude and direction of the relative distance between the ownship to the intruder, respectively.

$$\vec{D}_r(\omega, d_r, \theta_r, t) = \begin{bmatrix} d_r \sin\theta_r \\ d_r \cos\theta_r \end{bmatrix} + \int_0^t \vec{V}_r(\omega, t)dt \tag{2}$$

For any turn rate ω, the time for the ownship to arrive at the closest point of approach to the intruder will be the time that can minimize the relative distance, $\left\|\vec{D}_r\right\|$ (as shown in Eqn. 3). Newton's method can be utilized to find the time associated with the minimum. If there are multiple solutions, the minimum positive value should be chosen.

$$t^*(\omega, d_r, \theta_r) = \min\Big\{ \underset{t\in[0,2\pi/\omega)}{\operatorname{argmin}} \left\|\vec{D}_r(\omega, d_r, \theta_r, t)\right\| \Big\} \tag{3}$$

When a conflict is about to occur, the closest safe distance to the intruder only happens when the ownship takes the maximum left ($-\omega_{max}$) or right turn rate (ω_{max}), assuming the intruder maintains its original course. The closest safe distance can be selected from these two extreme turns using Eqn. 4:

$$\rho(d_r, \theta_r, \omega_{max}) = \max\left\{\left\|\vec{D}_r(-\omega_{max}, d_r, \theta_r, t^*(-\omega_{max}, d_r, \theta_r))\right\|, \left\|\vec{D}_r(\omega_{max}, d_r, \theta_r, t^*(\omega_{max}, d_r, \theta_r)\right\|\right\} \tag{4}$$

A simple root-finding algorithm like the Bisection method can be applied to find the minimum safe distance to the intruder, d_r^*, which can make the closest distance to the intruder, ρ, equal to the minimum separation, R_{min}. By including initial setting of v_o, v_i, ψ_i, and ψ_o as arguments on the left side and assuming the relative heading angle $\psi_r = \psi_o - \psi_i$, the closest distance can then be written as:

$$d_r^*(\theta_r, v_o, v_i, \psi_i, \psi_r, \omega_{max}, R_{min}) = \operatorname{argmin}\left\{\left\|\rho(d_r, \theta_r, \omega_{max}) - R_{min}\right\|\right\} \tag{5}$$

The set s, which contains d_r^* for all relative position angle θ_r, then forms the minimum safe operational boundary around the intruder for given v_o, v_i, ψ_i, ψ_r, and R_{min}. Since the maximum turn rate of the ownship aircraft is essentially decided by the aircraft speed v_o and its maximum bank angle ϕ_{max}, the set s can be expressed as:

$$s(v_o, v_i, \psi_i, \psi_r, \phi_{max}, R_{min}) = \left\{d_r^*(\theta_r, v_o, v_i, \psi_i, \psi_r, \phi_{max}, R_{min}),\ \forall\theta_r \in [0, 2\pi)\right\} \tag{6}$$

Finally, the set S then forms the aggregated minimum safe operational boundary around the intruder for the ownship coming from any direction (ψ_r) around the intruder, given a set of v_o, v_i, and R_{min}:

$$S(v_o, v_i, \psi_i, \phi_{max}, R_{min}) = \left\{s(v_o, v_i, \psi_i, \psi_r, \phi_{max}, R_{min}),\ \forall\psi_r \in [0, 2\pi)\ \right\} \tag{7}$$

2. Demonstration with three different pairwise encounters

Several typical pairwise encounter examples are presented to demonstrate the proposed algorithm. Fig. 2 presents a pairwise encounter between a balloon and a fixed-wing Global Hawk aircraft, where the balloon is static and the Global Hawk flies at 340 kts with a maximum bank angle of 14.8°. Fig. 3 shows an example between a HALE high aspect ratio aircraft and a Global Hawk, where the HALE aircraft cruises at a speed of 60 kts. In these two scenarios, the minimum separation R_{min} (represented by red circles around the balloon and HALE, respectively) is set to 3 nmi.

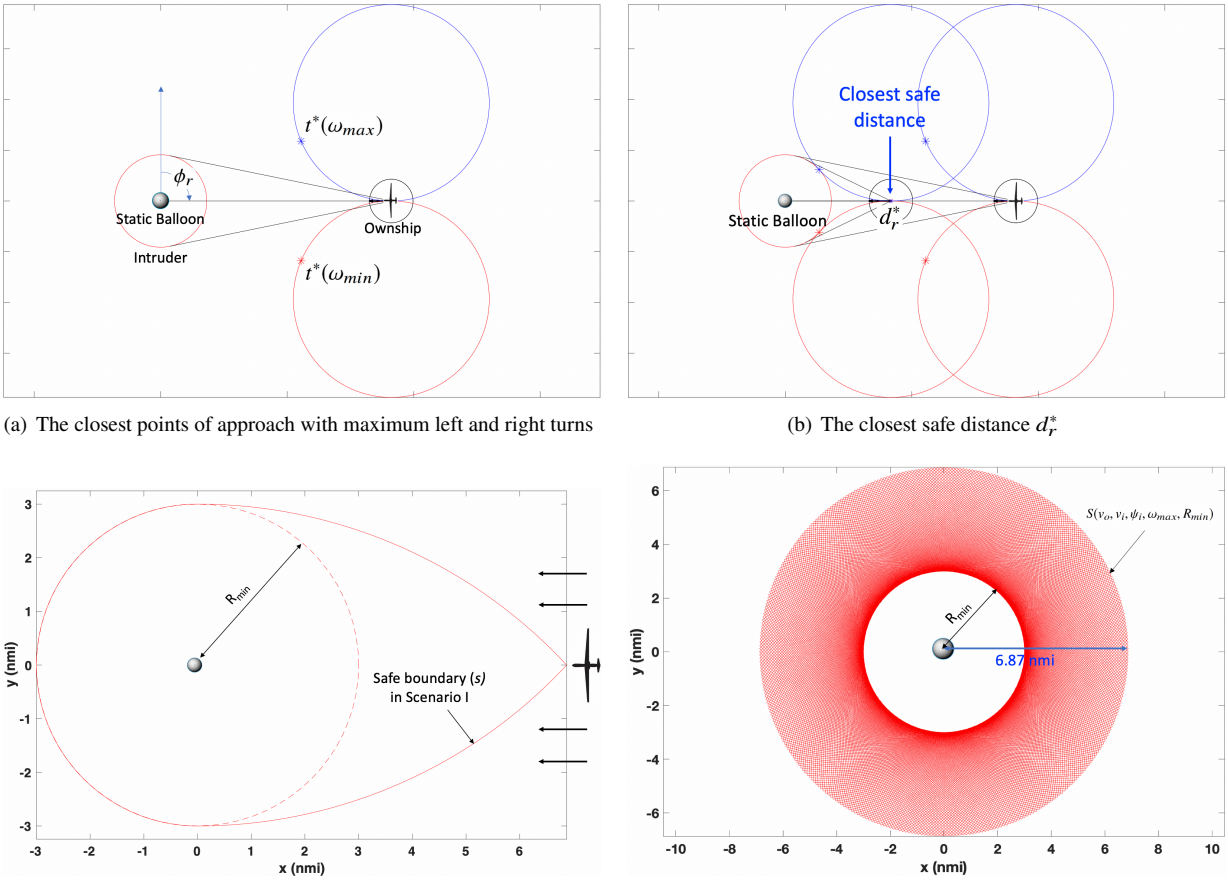

(a) The closest points of approach with maximum left and right turns

(b) The closest safe distance d_r^*

(c) The minimum safe operational boundary s for a given ψ_r

(d) The aggregated minimum safe operational boundary S for all ψ_r

Fig. 2 Scenario I: $v_i = 0$ kts, $v_o = 340$ kts, $\psi_r = -90°$, $\phi_{max} = 14.8°$, and $R_{min} = 3.0$ nmi

The times to the closest point of approach, $t^*(\omega_{max})$ and $t^*(-\omega_{max})$ calculated using Eqn. 3 are marked in Figures 2(a) and 3(a). $t^*(\omega_{max})$ is the time when the Global Hawk is taking a right turn with the maximum bank angle and $t^*(-\omega_{max})$ corresponds to the time when a left turn with the maximum bank angle is taken. Figures 2(b) and 3(b) show the resultant closest safe distances d_r^* calculated using Eqn. 5, which refers to the closest distance the Global Hawk can be before it can avoid the intruder with the maximum turn rate. When the intruder is nonzero as in Fig. 3(b) in Scenario II, the closest distance happens when the ownship turns right because a right with the maximum turn rate allows the ownship to stay closer than a left turn.

The boundary s for all relative position angle θ_r at a given relative heading angle ψ_r can then be computed using Eqn. 6 for each scenario and the boundaries are shown in Figures 2(c) and 3(c) for Scenario I and II, respectively. Fig. 2(c) shows that when the Global Hawk aircraft is heading towards the balloon, a minimum separation of 6.87 nmi is required due to the maximum bank angle limit (ϕ_{max}) of the Global Hawk. Since the speed of the high aspect ratio aircraft in Scenario II is still pretty slow, the boundary s in Scenario II is close to the one in Scenario I. To show the difference between these two, Fig. 3(c) puts them together with the blue and red curves representing s in Scenario II and I, respectively.

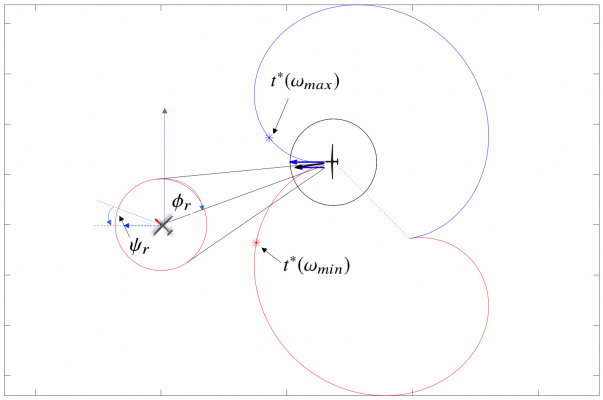

(a) The closest points of approach with maximum left and right turns

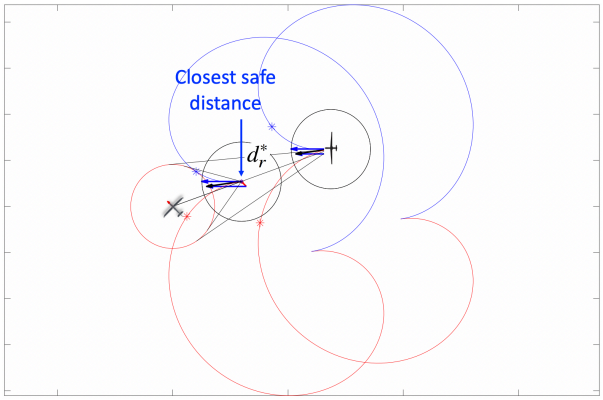

(b) The closest safe distance d_r^*

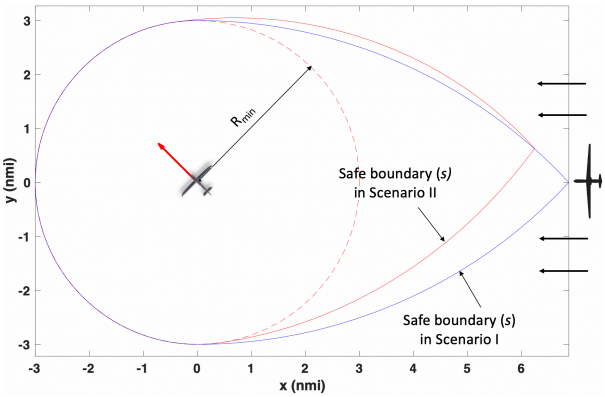

(c) The minimum safe operational boundary s for a given ψ_r

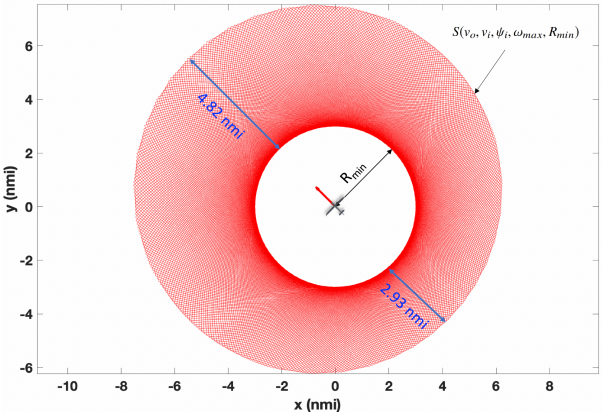

(d) The aggregated minimum safe operational boundary S for all ψ_r

Fig. 3 Scenario II: $v_i = 60$ kts, $v_o = 340$ kts, $\psi_r = -30°$, $\phi_{max} = 14.8°$, and $R_{min} = 3.0$ nmi

Given v_o, v_i, ψ_i, ϕ_{max}, and R_{min}, if the ownship is assumed to come from any direction (ψ_r), an aggregated minimum safe operational boundary S can be calculated using Eqn. 6. Figures 2(d) and 3(d) present such aggregated minimum safe operational boundaries for Scenario I and II, respectively. In Scenario I, since the balloon is static, the S is essentially a circle (a cylinder if considering a constant vertical separation) with the radius of 6.87 nmi, which means the 14.8° bank angle limit needs 3.87 nmi extra separation buffer. When the intruder speed is nonzero, the extra separation caused by the limited maneuverability increases when two vehicles fly in the opposite direction. And the extra separation decreases when the ownship trails the intruder as shown in Fig. 3(d). The aggregated boundary S is conservative and assumes the relative heading is unknown, however, the boundary s should be applied when both aircraft headings are certain. On the other hand, if aircraft headings are not deterministic, a probabilistic boundary can also be derived based on the Eqn. 6.

When two aerial vehicles are flying at similar speeds, the situation becomes a bit complex. However, the proposed method can be simply applied to calculate the boundaries. Scenario III presents an encounter scenario with two aircraft flying at 120 knots with $R_{min} = 1,200$ ft and the maximum bank angle $\phi_{max} = 25°$. Using Eqn. 3, the minimum positive times computed for ω_{max} and ω_{min} are the times to the closest point of approach, $t^*(\omega_{max})$ and $t^*(-\omega_{max})$, respectively, as shown in Fig. 4(a). The closest safe distances d_r^* can then be identified (Fig. 4(b)). The boundary s for all relative position angle θ_r at the same relative heading angle ψ_r is shown in Fig. 4(c). If the heading of ownship aircraft is unknown, Fig. 4(d) presents the aggregated minimum safe operational boundary. It's noted that when the ownship aircraft is trailing the intruder, no extra separation is needed for the limited maneuverability, whereas the extra buffer reaches the maximum when two aircraft are heading towards each other.

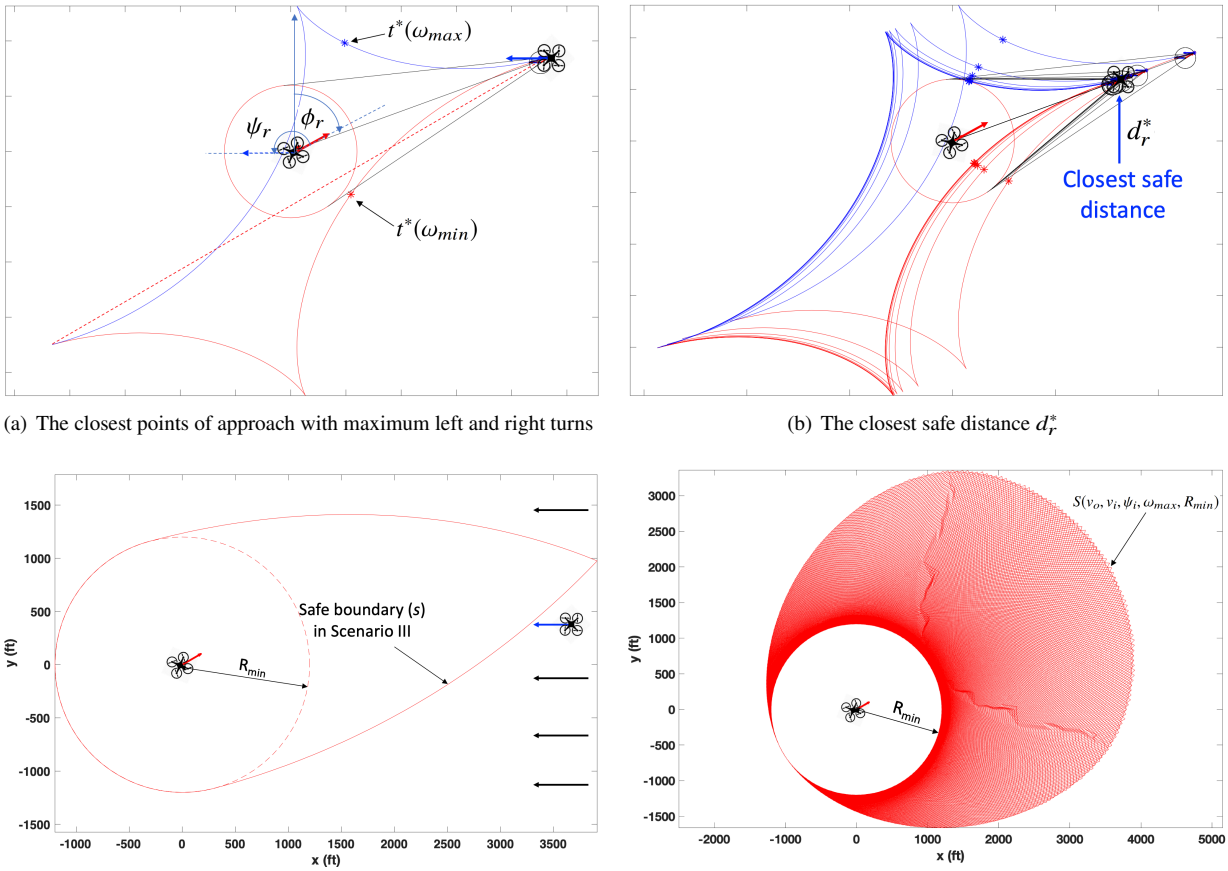

(a) The closest points of approach with maximum left and right turns

(b) The closest safe distance d_r^*

(c) The minimum safe operational boundary s for a given ψ_r

(d) The aggregated minimum safe operational boundary for all ψ_r

Fig. 4 Scenario III: $v_i = v_o = 120$ **kts,** $\psi_r = -150°$**,** $\phi_{max} = 25°$**, and** $R_{min} = 1,200$ **ft**

B. Separation required by delays caused by information update interval and control response

The information update interval refers to the time between two consecutive intruder positions/states acquired by the ownship. There are many approaches to acquire the intruder's positions/states, including air-to-air communications, air-ground-air communication, onboard sensor, and ground surveillance system. Regardless of the approach used for information acquisition, the model for calculating the resultant extra separation can be simply the product of the relative velocity vector $\vec{v_r}$ and information update interval τ_i as in Eqn. 8. When v_r, θ_r, and τ_i are all deterministic, the S' simply expands S at the direction of relative velocity as in Eqn. 8. If any or all of v_r, θ_r, and τ_i are uncertain, a preliminary probabilistic model can be derived based on Eqn. 8.

$$S'(\tau_i) = \begin{bmatrix} v_r \sin\theta_r \\ v_r \cos\theta_r \end{bmatrix} \cdot \tau_i \tag{8}$$

The other factor is the control response time, defined as the time needed from when information is acquired to when a resolution is executed by the ownship aircraft. It includes the time needed for the decision-making process and control response, from an onboard pilot, a remote pilot/operator, or an autonomous onboard/remote control system. Similar to the information update interval, the extra separation S'' needed by this factor is simply the product of the relative velocity vector $\vec{v_r}$ and the control response time τ_c as in Eqn. 9.

$$S''(\tau_c) = \begin{bmatrix} v_r \sin\theta_r \\ v_r \cos\theta_r \end{bmatrix} \cdot \tau_c \tag{9}$$

Although the update interval and control response delay are two different factors and are discussed separately, their impacts are essentially the same, which is introducing delays. The information update interval introduces delays in the information acquisition process, while the control response introduces delays in the decision-making and execution process.

III. Sensitivity analysis

As discussed in the previous section, the minimum safe operational boundary is affected by multiple parameters. For maneuverability alone, there are already five parameters including v_o, v_i, ψ_i, ψ_r, ϕ_{max}, and R_{min}. In order to gain a better understanding of the impact of these parameters, sensitivity analysis is conducted using the proposed algorithm. A simple encounter scenario with a stationary balloon as the intruder is used for this sensitivity study. Factors investigated in this section are the speed of the ownship aircraft v_o, the maximum allowable bank angle of the ownship ϕ_{max}, the minimum separation R_{min}, and the time delays due to information update interval and control response.

A. Sensitivity to the speed of ownship aircraft v_o

Fig. 5 shows the boundary s needed when the maximum allowable bank angle is fixed at 25°. The speed of the ownship aircraft shown in this figure varies from 340 knots to 2.0 Mach at FL600 representing the speed range of possible fixed-wing aircraft in future upper Class E airspace. It is noticed that when the ownship aircraft is flying directly towards the balloon, the extra separation distance (distance between the tip of the boundary to the dashed circle) required by the limited maneuverability of the ownship aircraft, can be anywhere between 2.54 nmi and 13 nmi in addition to the minimum separation. For instance, for a supersonic commercial aircraft flying at 2.0 Mach, it would need 16 nmi to stay clear from the balloon, assuming it can take a turn with a 25° bank angle. Fig. 6(a) depicts the extra separation needed (at the tip of the boundary shown in Fig. 5) from a different perspective, which reveals a quasi-linear relationship between the extra separation and v_o given the specific setting in this study. As a reference, the dashed lines represents a linear relationship.

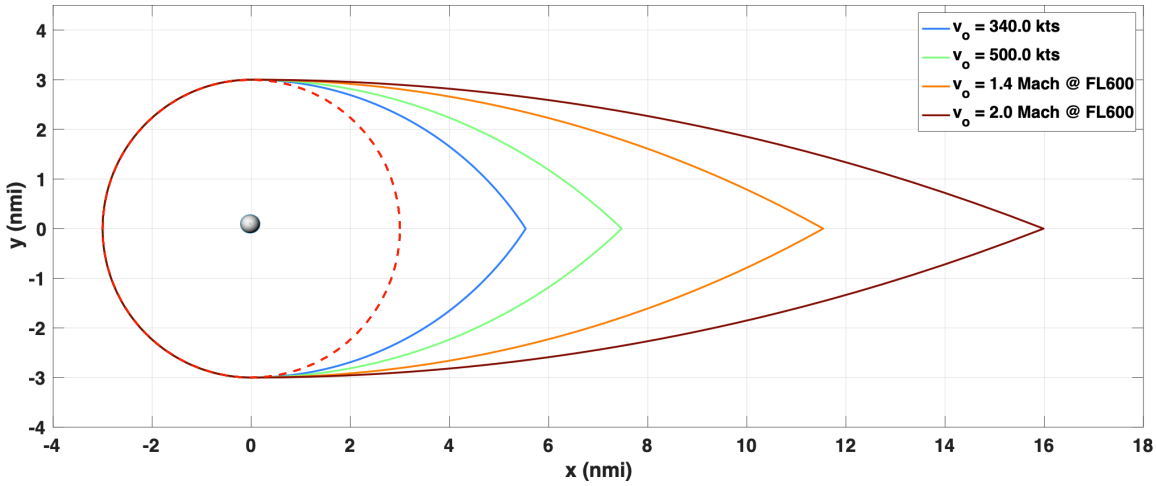

Fig. 5 Minimum Safe Operational Boundary s with varying v_o @ $\phi_{max} = 25°$

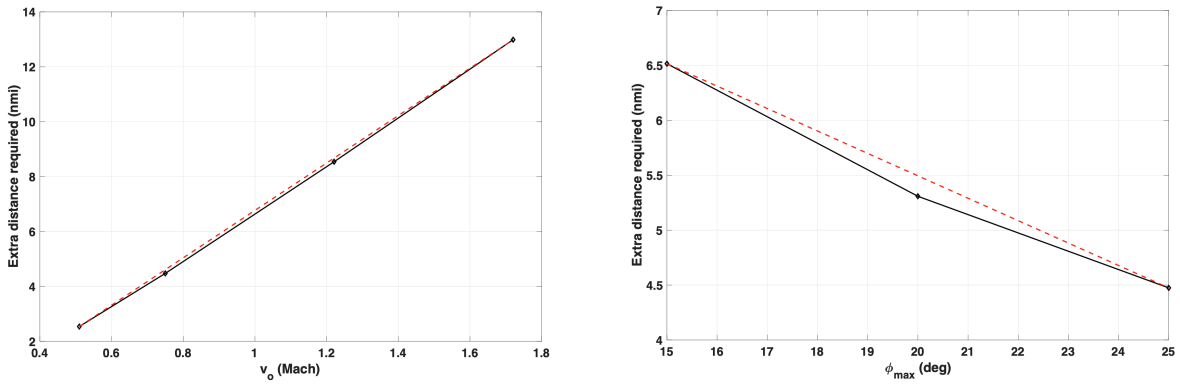

(a) Sensitivity to v_o (b) Sensitivity to ϕ_{max}

Fig. 6 The sensitivity of extra separation needed for maneuverability to v_o and ϕ_{max}

B. Sensitivity to the maximum bank angle ϕ_{max}

With the speed of ownship aircraft fixed at 500 kts, Fig. 7 shows the safe boundary s when the maximum allowable bank angle changes from 15° to 25°. The extra separation needed for the limited maneuverability will be 4.5 nmi if the ownship can take a 25° turn. Whereas the extra separation required by a 15° turn would be 6.5 nmi. Fig. 6(b) shows that the relationship between the extra separation needed for the limited maneuverability and the bank angle is nonlinear.

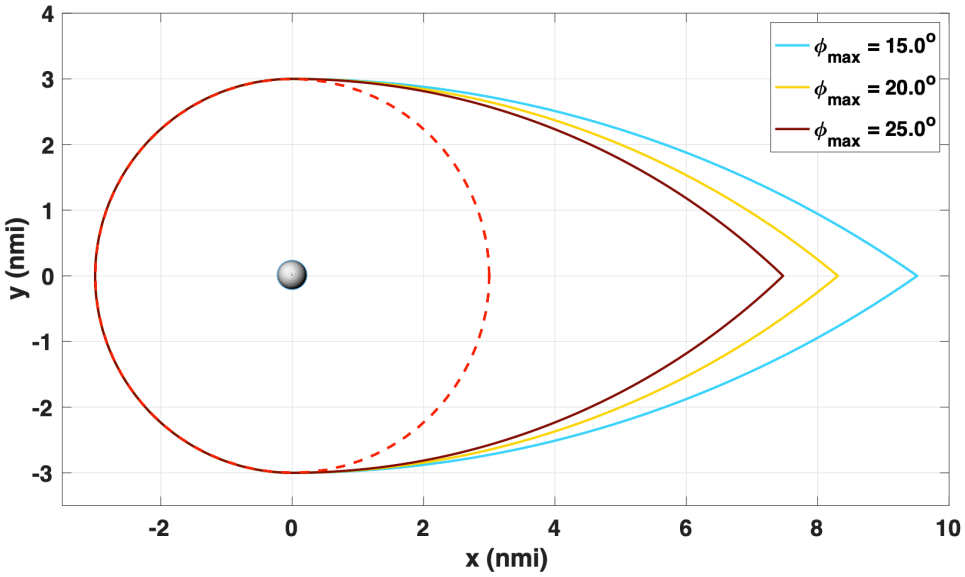

Fig. 7 Minimum Safe Operational Boundary s with varying ϕ_{max} @ v_o = 500 kts

C. Sensitivity to the minimum separation R_{min}

Fig. 8 shows the boundaries s when R_{min} is varied from 3.0 nmi to 8.0 nmi while keeping v_o at 500 kts and ψ_{max} at 25°. As expected the extra separation required by the limited bank angle increases with R_{min}. The extra separation seems to be proportional to the R_{min}. For instance, the extra separation is about 2.6 nmi when R_{min} is 3 nmi, and it increases to 8 nmi when R_{min} is 8 nmi. Fig. 9 reveals that the relationship between the extra separation and the minimum separation is close to but not purely linear (the dashed straight line in the figure serves as a reference).

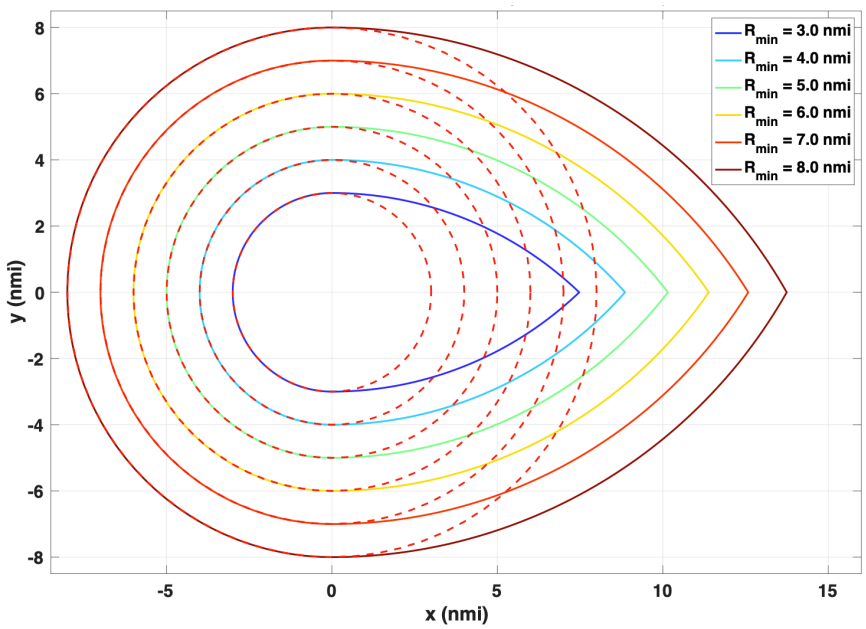

Fig. 8 The minimum safe operational boundaries with various R_{min}

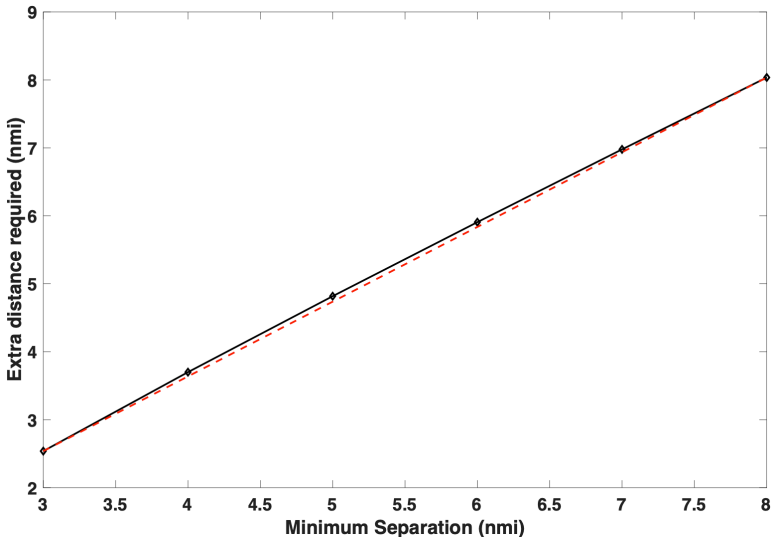

Fig. 9 Sensitivity to the minimum separation R_{min}

D. Sensitivity to delays caused by information update interval and control response

Both information update interval and control response time introduce time delays. Therefore the effects from both factors are essentially caused by time delay. Fig. 10 shows the linear relationship between the time delay (either caused by information update interval or control response time) and the extra separation needed for compensating for the time delay. The slope is essentially the ownship speed (as the intruder is a static balloon in this sensitivity study). If the time delay is 60 seconds, the extra separation needed for the delay is about 6 nmi.

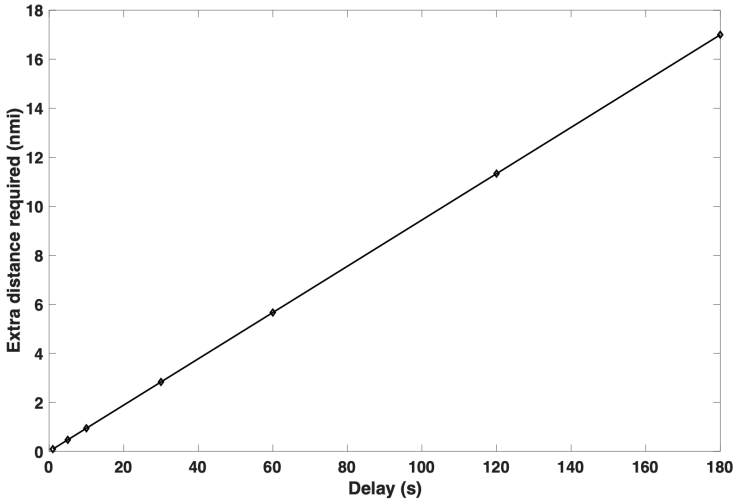

Fig. 10 Sensitivity to the delay caused by information update interval and/or control response

IV. Simulation

To verify the boundaries computed by the proposed analytical method, simulations are conducted for the selected encounter scenario between a balloon and a Global Hawk aircraft. The Fe^3 fast-time simulator [15] is utilized after new vehicle trajectory models were incorporated into the simulator.

A. Vehicle trajectory model

Two new vehicle trajectory models were developed in Fe^3 for the balloon and Global Hawk. The three-dimensional balloon only considers translational dynamics of the balloon with a proportional-integral controller to track the desired altitude. Similar to past works [16, 17], a kinetic point mass model was used for the Global Hawk, in which proportional and proportional-derivative controllers are used to track desired airspeed, horizontal path, and vertical profile. According to Global Hawk's dynamics [18], the bank angle was limited to 14.8° when the PD controller is trying to follow the desired horizontal heading.

B. Conflict detection and resolution

Fe^3 updates the trajectory every half second and generates conflict resolution or avoidance maneuvers (if needed) based on predefined rules or logic. In the experiment, the Global Hawk is assigned to be responsible to avoid any detected conflict and heading angle change is the only available resolution maneuver option. The parallel computing mechanism in Fe^3 allows the Global Hawk to check all possible heading changes and select a heading change that can avoid the detected conflict but have the minimum deviation from the original path. This conflict detection and resolution process also happens every half second.

C. Experiment setup

Thousands of pairwise encounters between a balloon and a Global Hawk are created. The balloon is assumed to be floating statically at the origin of the coordinates. The Global Hawk is set to fly towards the west at 340 kts starting from different locations relative to the balloon. In each pairwise encounter, the Global Hawk is assumed to start from one grid point shown in Fig. 11 (near the boundary computed using the proposed algorithm) and head towards the west. Therefore, the only varying independent variable is the initial location of the Global Hawk. These locations are selected by changing the relative direction (every 1°, 2°, or 5°) and relative distance (10 at each direction) around the boundary calculated using the proposed method. The total number of these initial locations is 1,166, as shown in Fig. 11.

D. Experiment results

Simulation results of these 1,166 encounters are shown in Fig. 12. If the Global Hawk failed to keep the minimum separation (the dashed circle), its initial location is then marked as a red point. Fig. 12 shows that when the Global

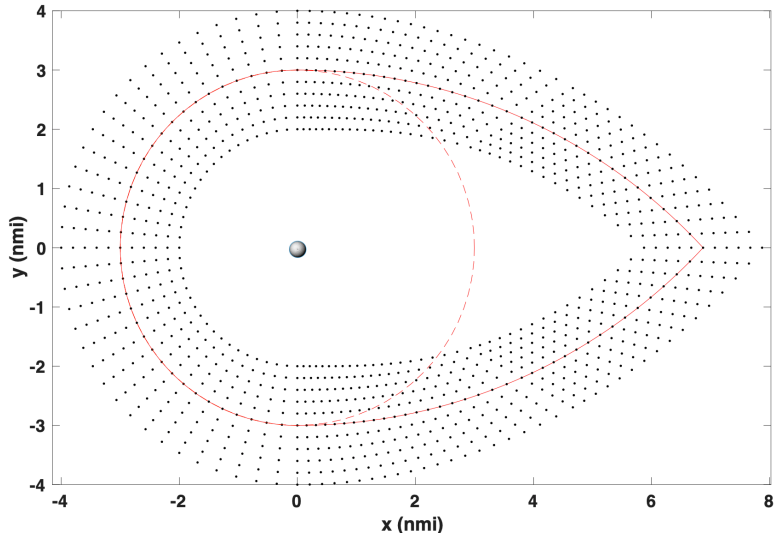

Fig. 11 Encounters with the balloon at the origin and the Global Hawk at different initial location

Hawk starts from any location within the calculated boundary and flies towards the west, the minimum separation will be violated. Whereas if the Global Hawk starts from any initial locations outside the boundary, it then can maintain the minimum separation by turning left or right. Among the safe initial locations, if the left turn was taken by the Global Hawk to stay out of the separation violation, that location is in green. If the right turn was taken to avoid the loss of separation, the initial location is in blue. If the Global Hawk starts from initial locations with the magenta color, it then has both left turn and right turn options to keep the minimum separation. One may note that when the initial location is on the boundary, the results showed that the Global Hawk can maintain minimum separation if it is on the right side of the balloon. That is caused by the setup of the Fe^3 simulator, which only starts to check for conflict after the first half second. Overall, the simulation experiments show that the boundary calculated by the proposed algorithm is accurate.

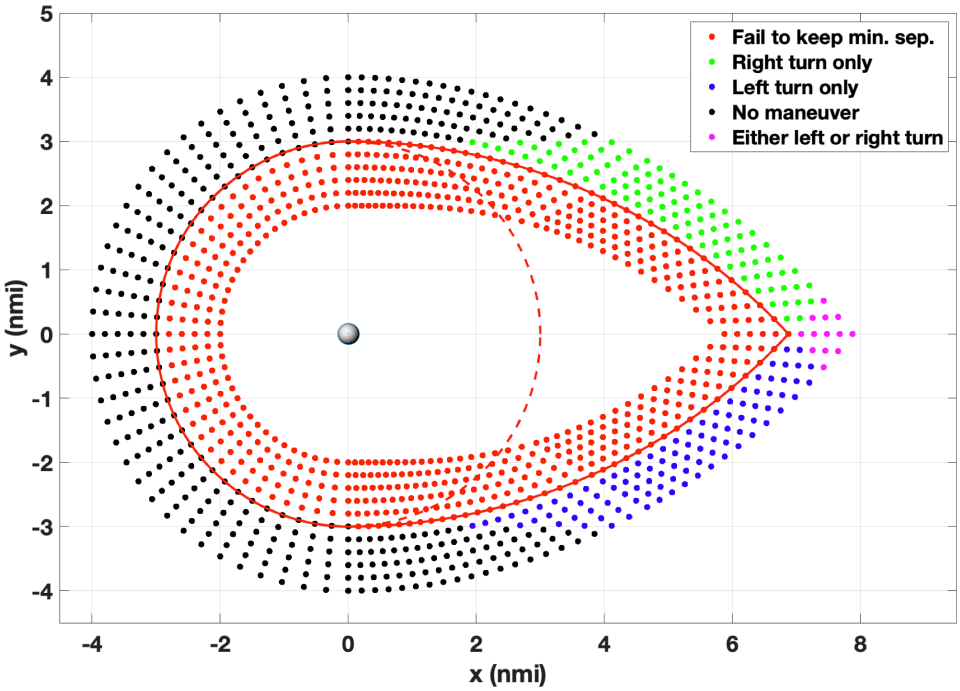

Fig. 12 Results of encounter scenarios with the Global Hawk at different initial locations

V. Conclusions

High altitude operations above FL600 allow broader service area coverage than at ground level and have attracted many commercial applications. Balloons, airships, high-altitude long-endurance (HALE) aerial vehicles, and supersonic aircraft have been developed to provide platforms to enable these high-altitude operations. Defining the minimum safe operational boundary for disparate vehicles is a critical step to improve currently limited airspace management service in upper Class E.

This work presented a mathematical method to define the minimum safe operational boundary needed for aerial vehicles operating in upper Class E airspace. This method calculates the extra separation required by vehicle maneuverability, communication delay, and control/operator response time. A sensitivity study was performed to gain insight into the relationship between these factors and the extra separation needed. Simulation experiments with pairwise encounters were conducted for selected scenarios, and results verified the correctness of the safe operational boundary calculated by the proposed method.

References

[1] Bellemare, M. G., Candido, S., Castro, P. S., Gong, J., Machado, M. C., Moitra, S., Ponda, S. S., and Wang, Z., "Autonomous Navigation of Stratospheric Balloons using Reinforcement Learning," *Nature*, Vol. 588, 2020, pp. 77–88.

[2] "Sceye Inc. to Build Stratospheric Airships in NM," *Albuquerque Journal*, 2020. URL `https://www.abqjournal.com/1487318/sceye-inc-to-build-stratospheric-airships-in-nm.html`.

[3] "HAPSMobile's Sunglider Succeeds in Stratospheric Test Flight," *sUAS News*, 2020. URL `https://www.suasnews.com/2020/10/hapsmobiles-sunglider-succeeds-in-stratospheric-test-flight/`.

[4] Martin, R. A., Gates, N. S., Ning, A., and Hedengren, J. D., "Dynamic Optimization of High-altitude Solar Aircraft Trajectories Under Station-Keeping Constraints," *AIAA Journal of Guidance, Control, and Dynamics*, Vol. 42, No. 3, 2019, pp. 538–552.

[5] Dempsey, M., "New Jets Promise To Revive Supersonic Travel," *BBC News*, 2020. URL `https://www.bbc.com/news/business-54416696`.

[6] O'Hare, M., and Sillers, P., "Supersonic Airliner Could Fly LA to Tokyo in Under Three Hours," *CNN Travel*, 2021. URL `https://www.cnn.com/travel/article/aerion-as3-supersonic-jet/index.html`.

[7] *Upper Class E Traffic Management (ETM) Concept of Operations*, FAA, 2020. URL `https://www.faa.gov/uas/advanced_operations/upper_class_etm/`.

[8] Yoo, H., Li, J., Homola, J., and Jung, J., "Cooperative Upper Class E Airspace: Concept of Operations and Simulation Development for Operational Feasibility Assessment," *AIAA Aviation 2021*, Virtual, 2021.

[9] Wang, C., Baets, P., Fenkell, M., Tailby, A., Barry, S., Taylor, P., Bouygues, L., Mian, Z., Gentry, J., and Kluttz, B., "Adaptive Risk-based Conflict Detection for Stratospheric Flight Operations," *Air Traffic Control Association Tech Symposium*, Virtual, 2020.

[10] Wu, M. G., Cone, A. C., Lee, S., Chen, C., Edwards, M. W. M., and Jack, D. P., "Well Clear Trade Study for Unmanned Aircraft System Detect And Avoid with Non-Cooperative Aircraft," *AIAA Aviation 2018*, Atlanta, Georgia, 2018.

[11] Vincent, M., Trujillo, A., Jack, D., and Hoffler, K., "A Recommended DAA Well-Clear Definition for the Terminal Environment," *AIAA Aviation 2018*, Atlanta, Georgia, 2018.

[12] Weibel, R. E., Edwards, M. W. M., and Fernandes, C. S., "Establishing a Risk-Based Separation Standard for Unmanned Aircraft Self Separation," *Ninth USA/Europe Air Traffic Management Research Development Seminar*, Berline, Germany, 2011.

[13] Duffield, M. O., and McLain, T. W., "A Well Clear Recommendation for Small UAS in High-Density ADS-B-Enabled Airspace," *AIAA SciTech Forum*, Grapevine, Texas, 2017.

[14] Tomlin, C., Pappas, G. J., and Sastry, S., "Conflict Resolution for Air Traffic Management: A Study in Multiagent Hybrid Systems," *IEEE Transactions On Automatic Control*, Vol. 43, No. 4, 1998, pp. 509–521.

[15] Xue, M., Rios, J., Silva, J., Ishihara, A., and Zhu, Z., "Fe^3: An Evaluation Tool for Low-Altitude Air Traffic Operations," *AIAA Aviation Forum*, Atlanta, GA, 2018.

[16] Chatterji, G. B., Sridhar, B., and Bilimoria, K. D., "En-route Flight Trajectory Prediction for Conflict Avoidance and Traffic Management," *AIAA Guidance, Navigation, and Control Conference*, San Diego, CA, 1996.

[17] Chatterji, G. B., "Trajectory Simulation for Air Traffic Management Employing a Multirotor Urban Air Mobility Aircraft Model," *AIAA Aviation*, Virtual event, 2020.

[18] Pastor, E., Perez-Batlle, M., Barrado, C., Royo, P., and Cuadrado, R., "A Macroscopic Performance Analysis of NASA's Northrop Grumman RQ-4A," *Aerospace*, Vol. 5, No. 1, 2018, pp. 1–16.